RSC Advances




ROYAL SOCIETY OF CHEMISTRY

www.rsc.org/advances

Cite this: DOI: 10.1039/c0xx00000x

www.rsc.org/xxxxxx

COMMUNICATION

# High Transparent porous $ZrO_2$ thin films: fabrication and optical properties

**Yu Chen,** * [a, c] **Aolin Li,**[a] **Yige Li,**[a] **Junfei Li,**[a] **Guozhang Dai,**[a] **Ouyang Fangping,*** [a, c] **Xiang Xiong,**[b]

*Received (in XXX, XXX) Xth XXXXXXXXX 200X, Accepted Xth XXXXXXXXX 200X*

**DOI: 10.1039/b000000x**

**A novel two-step method is proposed to fabricate porous zirconia ($ZrO_2$) thin films. A large-scaled $ZrO_2$ thin film is thus achieved, which displays a very good light transparence for its total transmissivity higher than 95% within the wavelength of 450-1100 nm, a broad range just covered both the visible and near-infrared spectral range. This property makes it a promising candidate for solar cells as a high-temperature-resistant insulating layer.**

Zirconium dioxide ($ZrO_2$) thin films have attracted wide attentions due to their potential applications in catalysts, sensors and high-performance photoelectric devices [1-4]. $ZrO_2$ is the only traditional metal oxide having both acid and base active centers on its surface [5]. This makes $ZrO_2$ having many excellent physic-chemical properties such as good insulation, high refractive index and catalytic activity [6-8]. Especially in optics, the characteristics of both the high-temperature thermal stability and high transparency in the visible or near-infrared regions also indicate that it can be used in many photoelectric devices and transparent high-temperature-resistant insulating layers. For example, G. Sumana et al. reported a novel biosensor based on Au/$ZrO_2$ composite thin-film that has a high sensitive in urea testing [9]. Most recently, Anyi Mei et al. fabricated a perovskite solar cell that uses a $ZrO_2$ insulating layer connecting between $TiO_2$ nanocrystalline and carbon electrode [10]. They have finally achieved a long-term working stability and high light conversion efficiency [10]. Therefore, any approaches that could obtain high-quality $ZrO_2$ thin films are of great interests for these potential wide applications.

Many approaches so far have been developed to synthesize $ZrO_2$ thin films. These include the sol-gel method [11], chemical vaporous deposition (CVD) [12], self-assembly block copolymer templating method [13] and etc. Miko et al. used block copolymers as the template that fabricated a vertically orientated and long-range ordered mesoporous $ZrO_2$ thin film [13]. Chen et al. also reported a method that synthesized a high-performance mesoporous $ZrO_2$ thin film using Tween 20 as the structural directing agent [14]. These approaches above typically involve adding multiple surfactants and agents or requiring specific templates. Templates used in the fabrication, however, generally need a further step to remove the template. It is also a big task to clean-out all surfactants and agents in the end of the preparation.

In our present work, a simple sol-gel dip-coating method has been proposed to prepare high transparent porous $ZrO_2$ thin films which the process does not requires any additional surfactants and agents. Porous $ZrO_2$ has been pre-prepared via a directly decomposing of a $Zr(NO_3)_4 \cdot 5H_2O$ ethanol sol-gel solution. Then, mesoporous nanoparticles with the average size around 60 nm were purely isolated and stably dispersed in the ethanol solution using an ultrasonic separation and cleaning process. After the dip-coating step, a high transparent $ZrO_2$ thin film was finally obtained. Experimental clarifications of the optical transmission properties have shown a good transparence of the film for both the visible and infrared light. Furthermore, three possible models based on FDTD method were built to discuss the influence of various structure parameters of $ZrO_2$ thin films on light transmissions.

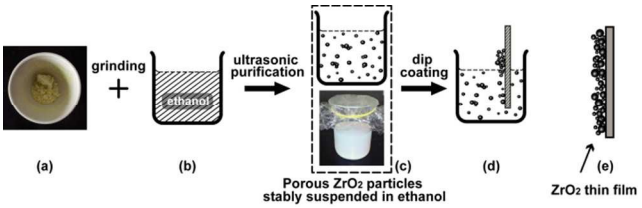


**Fig. 1** Schematic representation of the experimental procedure. (a) Porous $ZrO_2$ fluffy masses after the crystallization. It should be grinded into powder and further refined in order to meet the requirement for thin-film depositions. (b) Anhydrous ethanol. $ZrO_2$ prepared in the last step were dispersed into this solution and should be ultrasonically vibrated for another one hour. Certain particles with narrow size-distribution and high surface-area will be isolated and form a stable suspension of (c). (d) The dip-coating process. In this process, the concentration of $ZrO_2$ in the coating solution (c) can be adjusted accordingly and its influence on the film's thickness and uniformity can be clarified. (e) Randomly deposited $ZrO_2$ have finally formed a compact thin film on the silica substrate.

The entire fabrication process is illustrated in Fig. 1. Firstly, a simple gel-sol method was utilized to fabricate hierarchical porous $ZrO_2$ owning to its many advantages such as does not requires expensive organic pore-forming agents and other complex post-treating processes. The detailed descriptions of this method can be found in *Ref. 5*. Porous $ZrO_2$ achieved at this moment are loosely packed together in a fluffy mass. It should be grinded into powder and mixed with anhydrous ethanol for further purifications. In the purification process, the mixture was ultrasonic oscillated for about 1 hour and then left untouched until a stable and homogeneous suspension was obtained. This solution contains well separated and refined porous $ZrO_2$ that have a narrow-distributed particle size and considerable high surface area (The nitrogen adsorption/desorption data can be

found in *Ref 5*, which shows a high BET surface area over 162 $m^2 \cdot g^{-1}$). Secondly, the refined $ZrO_2$ particles after the purification have been examined by Transmission Electron Microscope (TEM) in order to investigate their morphology, particle size and dispersity.

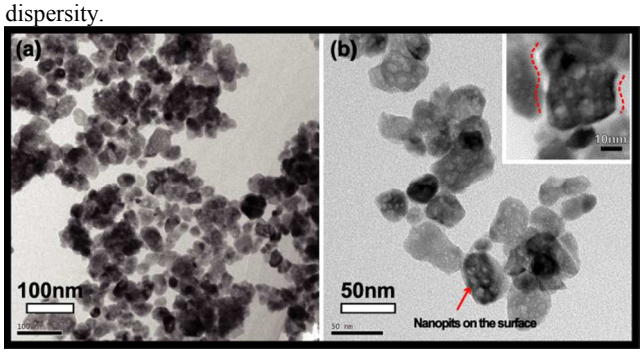


**Fig. 2** TEM images of the porous $ZrO_2$ nanoparticles dispersed in the coating precursor. (a) An image measured at a considerable low magnification which shows a good dispersity. (b) TEM result tested at a higher magnification which hemispherical nanopits spreading on the surface of $ZrO_2$ particles can be clearly identified. The inset in (b) is the HRTEM image of one-single $ZrO_2$ particle, which the sub-nanostructures of spherical nanopits can be observed. The dashed red line marked an irregular or wave-shaped edge which further confirms the existence of these nanopits.

Fig. 2 shows the results and illustrates a good dispersity. Furthermore, mesopores which are spherical and with average diameter around ~ 8 nm were founded spreading on the surface of each $ZrO_2$ nanoparticles (~ 60 nm). The inset of Fig. 2(b) gives a HRTEM image of one-single isolated porous $ZrO_2$ which exhibits a wave-like surface edge. This phenomenon confirms the existence of hemispheric nanopits full-filled on the surface of every $ZrO_2$ nanoparticles. Previously studies have reported that these nanopits were formed by $NO_2$ bubble-templates which were released in a fast decomposition of $Zr(NO_3)_4 \cdot 5H_2O$ sols [5]. The pore-forming process will also significantly improve the particle-surface-area. The detailed descriptions please refer to the ***Ref. 5***. The narrow particle size distribution, high surface area and good dispersity and stability of the coating solution is the key prerequisite for making high-quality of $ZrO_2$ thin films. Thus the current porous $ZrO_2$ fabrication and purification method can prepare a novel precursor for the next step of thin-film depositions.

In the dip-coating process, the concentration of coating precursors prepared in the last step have been adjusted to four different values of $\omega$ = 5, 10, 15 and 20 $\mu g \cdot mL^{-1}$ respectively. However, the substrate withdrawal speed is fixed at ~5$\mu m \cdot s^{-1}$ so as to investigate only those influences caused by variations of $\omega$. The temperature in the coating process at this time is 30 ºC. The fabricated thin films use these four conditions are labeled as sample I, II, III, IV respectively. Fig. 3 is the SEM images of the fabricated $ZrO_2$ thin films using the above-mentioned physical parameters. It can be inferred from these images that the films' quality is determined crucially by $\omega$ (the concentration of $ZrO_2$ in the coating solution). When this value is lower than 5$\mu g \cdot mL^{-1}$, we can only obtain a loosely distributed $ZrO_2$ grains on silica substrate instead of a compact thin-film (See Fig. 3(a)). However, a little segregation happened when $\omega$ is larger than 15$\mu g \cdot mL^{-1}$ (See Fig. 3(c)). The red dashed circles in Fig. 3 (d) marked two aggregated $ZrO_2$ particles which have owned a larger particle size than their nearby counterparts. Surface defects are also increased with the increase of $\omega$. The blue rectangles in Fig. 3 (d) have shown some hole-defects in the fabricated thin films which confirmed this assumption. In fact, there are also some hole-defects in sample II (See Fig. 3 (b)), but their distributions, either hole size or locations, is more homogeneous than those in sample III and IV (See Fig. 3 (c) and (d)). SEM tested results have indicated that the best $ZrO_2$ concentration for the film deposition is around 10 $\mu g \cdot mL^{-1}$ (See the SEM images of sample II in Fig. 3 (b)).

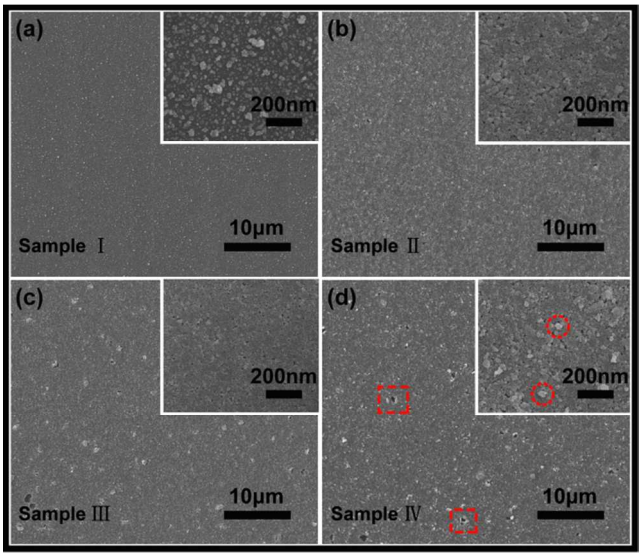


**Fig. 3** SEM investigations of the as-synthesized $ZrO_2$ thin-films. It was measured without the high temperature annealing. (a) Sample I, $\omega$ = 5$\mu g \cdot mL^{-1}$. The inset shows that well-refined $ZrO_2$ nano-particles were homogeneously deposited on the substrate. But owning to the very low concentration of $\omega$, compact thin-film have not yet been completely shaped; (b) Sample II, $\omega$ = 10$\mu g \cdot mL^{-1}$. The result shows a very good uniformity and surface conditions; (c) Sample III, $\omega$ = 15$\mu g \cdot mL^{-1}$. A little aggregation will happen at this concentration; (d) Sample IV, $\omega$ = 20$\mu g \cdot mL^{-1}$. Besides particle aggregation, lots of hole-defects have been detected. The dashed rectangle and circle marked some hole-defects and aggregated $ZrO_2$ particles respectively.

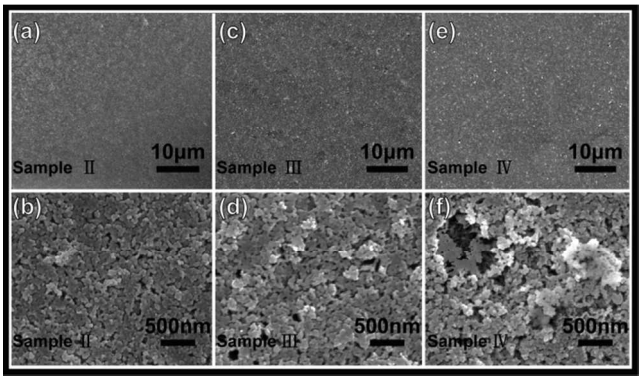


**Fig. 4** SEM images after the annealing. (a-b) Sample Ⅱ; (c-d) Sample Ⅲ; (e-f) Sample IV.

Fig. 4 (a)-(c) is the film after the annealing which is corresponding to Fig. 3 (b)-(d). $ZrO_2$ nanoparticles in Fig. 3 (b)-(d) are stacked and loosely bonded by weak van der Waals forces. This weak interaction determined that they are easy to fall off from the silica substrate unless they are properly annealed at the

high temperature. The annealing, however, can enhance the adhesion of $ZrO_2$ on the silica substrate. In fact, the $ZrO_2$ gels after the fast decomposing of $Zr(NO_3)_4$ has once been annealed at different temperature before the thin film deposition. The XRD data can be found in the Supplementary Appendix. The results have shown that tetragonal crystalline $ZrO_2$ can be achieved if the sintering temperature is higher than 400 ºC. Thus, in order to enhance the film-to-substrate adhesion, the film has been annealed again at 500 ºC. The Appendix also contains supplementary XRD materials for $ZrO_2$ thin films before and after that annealing (Supplementary data, Fig. S1). It suggests that there is no notable difference of the XRD data for the film before and after the annealing. However, it is interested to found that the film shows a high [011] orientation. This phenomenon will be discussed elsewhere in our other related works. Fig. 4 (a)-(c) is the SEM images at a very low magnification which shown no distinct particle aggregations and heat-treatment-induced cracks on the film surface. After the annealing, $ZrO_2$ particles have been grown up and became more compact (See Fig. 4 (d)-(f)). However, the size of the hole-defects is reduced owning to the shrinkage during the high temperature.

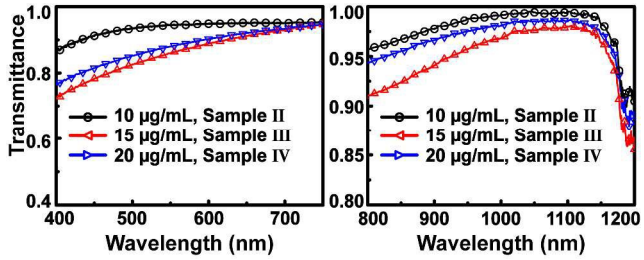


**Fig. 5** Transmission spectra of $ZrO_2$ thin-films. (a) The result measured at visible wavelength range; (b) The result measured at near-infrared wavelength range which also shows a high transparence.

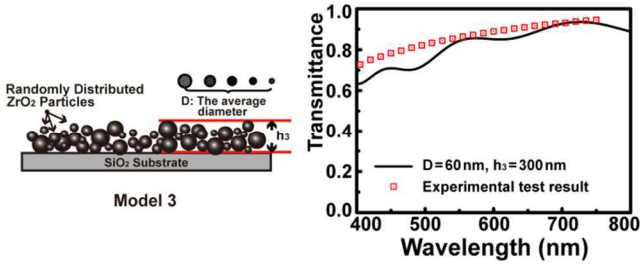


**Fig. 6** FDTD simulation results. Model 3, a disordered structure which was composed of randomly distributed ZrO2 particles. D is the average particle diameter, whereas h3 is the film' thickness.

As a good insulting layer applied in solar cell system, it requires high transmission, high thermal resistance and good electrical insulation. Fig. 5 shows the transmission spectra measured on a Vis/NIR spectroscopy which the transmission properties can be identified. The results have shown that all $ZrO_2$ thin films are found to be highly transparent to both the visible and infrared light. The sample II showed the best optical properties for its total light transmission higher than 95% within a broad wavelength ranged from 450-1100 nm. $ZrO_2$ is a traditional high-temperature resistant material having very good electrical insulation stability. Thus, the synthesized porous $ZrO_2$ thin film in this experiment is suppose to have the potential wide applications in solar cell systems.

Finally, we built three simple models to theoretically analyze the main factors that determined the high and broad range of achieved transparence. The structure models have been schematically illustrated in Fig. 6 and Supplementary data Fig. S2.

**Model 1:** the film surface is considered to be exactly smooth (Supplementary data, Fig. S2 model 1). In this model, it believes that the $ZrO_2$ particles are tightly stacked and their sizes are too small to be resolved by the visible light. We change the films' thickness to calculate its influence on the transmission spectra. The results shown many transmittance peaks within 400-800nm. The number of peaks is decreased and the half peak width became wider with the increase of the film thickness $h_1$. Previous researches indicate that these peaks are induced by the interference of waves reflected from the top and bottom surface [15]. The simulated results are quite different from the tested ones which implied that this model can't truly reflect the surface conditions of the fabricated $ZrO_2$ thin films.

**Model 2:** it is a cubic close-packing model which composed of orderly stacked spherical $ZrO_2$ particles. Each sphere has the same diameter. In this model, the number of layers is kept unchanged. The calculated results of the transmission spectra are displayed in Fig. S2 (b). It is also different from the experimental tested results because there are some transmission dips with its intensity lower than 60%.

**Model 3:** it is a disordered structure composed of randomly distributed $ZrO_2$ particles with which their particle sizes ranged within 20-80 nm. The structure was built by three steps. First, we supposed that the particle were spherical and close packed as shown in Fig. S3. Every square cell thus contains one single spherical $ZrO_2$ nanoparticle in its center. Then the coordinate of the center point of every $ZrO_2$ was changed. Its value was randomly produced by the computer, but it should be confined within the square cell. Also, the diameter of $ZrO_2$ was varied from 20 to 80 nm accordingly. After these transformations, a series of belts which composed by randomly distributed $ZrO_2$ particles are achieved (Fig. S3 step 2 shows one of these belts). Finally, we randomly stacked these $ZrO_2$ belts layer by layer to form a disordered film structure (see Fig. S3 step 3). It should be pointed out that this is still an approximate structure. However, it is thought to be more representative to the real conditions according to the SEM investigations. The simulated result is more qualitative agreement with the experimental tested results compared to **Model 1** and **2**. While the average particle size is around 60 nm, the film thickness is less than 300 nm and the film is composed of randomly distributed $ZrO_2$ particles, the simulated result shows a good qualitative agreement with the experimental tested results. The simulation result confirms that the main factors of the transmission spectrum are the particle size, film thickness as well as their distributions (stacked modes). There is still a little difference between the experimental test results and the theoretical calculated ones. The main reason can be concluded as the following two aspects. Firstly, the edge of particles is irregularly varied instead of a regular sphere in the simulations. Secondly, structural model in the simulation is a two-dimensional one which means disorders are only existed in one direction. But in fact, the film is a plane. Thus, disorders should be along with two directions. These differences will inevitably cause deviations

between the experimental test results and the theoretical calculated ones.

In summary, a novel and simple approach has been proposed for preparing high transparent porous $ZrO_2$ thin films. The film thickness, uniformity and its transparence can be well control by adjusting the concentration of porous $ZrO_2$ particles in the coating solution. SEM images have shown that there is a relative good quality, either flatness or uniformity, while the concentration for the film deposition is around 10 $\mu g \cdot mL^{-1}$. Final FDTD simulations are help to confirm what has been achieved in the experimental characterizations. The fabricated thin film is found to be highly transparent in both the visible and infrared wavelength range, promising wide potential application in solar cell systems as a high-temperature resistant insulting layer.

## Methods

**The preparation of the porous $ZrO_2$**

The key factor that determines the film's quality is its constituent material of $ZrO_2$ nanoparticles. It commonly requires high purity, good dispersity, narrow particle size distribution and etc. Thus, the porous $ZrO_2$ nanoparticles required for dip-coatings were synthesized by a simple sol–gel process which does not need any complicated procedure or additional surfactants. The used regents of $Zr(NO_3)_4 \cdot 5H_2O$ and alcohol were analytic grade, purchased from Sinopharm Chemical Reagent Changsha Co. Ltd. Firstly, 20 g $Zr(NO_3)_4 \cdot 5H_2O$ powder was mixed with 60 mL of anhydrous ethanol at room temperature to form an emulsion. It was then heated up to 40 ºC with constant stir until it becomes transparent and had completely dissolved. After that, it was slowly heated up to 60 ºC just a little lower than its boiling point and volatilizing at this temperature to achieve a high concentration. When this gel-sol solution started to get viscous (total concentration is more than 90%), the temperature was heated up quickly to 90 ºC. Along with this progress, a large amount of $NO_2$ tawny gas was released and was utilized as a pore-forming template to generate hierarchical porous $ZrO_2$. The achieved $ZrO_2$ gels were further dried in the air for another 2 hours and then transferred to a muffle furnace for the crystallization. The heating speed is 4 ºC /min, then kept at 600 ºC for 2 hours and finally cooled naturally in the ambient air.

**The dip-coating process to fabricate porous $ZrO_2$ thin films**

The dip-coating procedure is described in Fig. 1. After the crystallization, hierarchical porous $ZrO_2$ are loosely packed together in a fluffy masse. This material should be firstly grinded into powder, and then mixed with ethanol for the next step of the separation and purification. Porous $ZrO_2$ with a high surface area and narrow-distributed particle size around 20~80 nm will be separated after 2 mins ultrasonic vibration and left untouched for another 24 hours. Large-sized $ZrO_2$ particles will be deposited on the bottom of the vessel leaving refined particles suspending homogeneously in the ethanol (please see the picture differentiated by the dashed rectangle in Fig. 1). Using this method, we can isolate 50 mg highly refined porous $ZrO_2$ particles from every 10 g raw material. Then, the content $\omega$ of $ZrO_2$ in the coating solution is adjusted to 5, 10, 15, 20 $\mu g \cdot mL^{-1}$ respectively. However, the coating withdrawal speed is the same ($v$ = 10 $\mu m \cdot s^{-1}$) for these four $ZrO_2$ content conditions. Finally, the fabricated $ZrO_2$ thin films were annealed again at 500 ºC for 2 hours. The purpose of this annealing is to further improve the film-to-substrate adhesion.

The synthesized $ZrO_2$ after annealing at different temperatures were examined by X-ray diffraction (XRD) measurements on a D/max-2550/PC instrument with a scanning speed of 2 degrees/minute (see Fig. S1). The isolated porous $ZrO_2$ particles suspending in the ethanol has been examined by HRTEM (High-resolved Transmission Electron Microscopy). The measurements were taken on a JEM-2100f instrument under an acceleration voltage of 200 kV. FESEM (Filed Emission Scanning Electron Microscope) tests were operated on an FEI Sirion 200 to character the surface morphology of $ZrO_2$ thin films. The light transmission properties were analyzed using a visible/near-infrared spectroscopy (Vis/NIR spectroscopy, Ocean Optics HR4000).

## Acknowledgements

This work is financially supported by the National Science Foundation of China the (no. 61405260), the Distinguished Young Scholar Foundation of Hunan Province (no. 2015JJ1020) and Hunan provincial Natural Science Foundation of China (no. 13JJ3005). We greatly appreciate the support from Instrumental Analysis Center of Central South University, Changsha, P.R. China.

## References

[a] *School of Physics Science and Electronics, Central South University, 932 Lushan Nan Rd., Changsha, Hunan 410083, P.R. China; E-mail: chenyu_8323@csu.edu.cn; Ouyangfp06@tsinghua.org.cn*

[b] *Powder Metallurgy Research Institute, and State Key Laboratory of Powder Metallurgy, 932 Lushan Nan Rd., Changsha, Hunan 410083, P.R. China;*

[c] *Department of Electrical Engineering and Computer Science, Massachusetts Institute of Technology, 77 Massachusetts Avenue, Cambridge Massachusetts 02139, United States;*

† Electronic Supplementary Information (ESI) available:

1. H. Xie, J. Lu, M. Shekhar, J. W. Elam, W. N. Delgass, F. H. Ribeiro, E. Weitz and K. R. Poeppelmeier, *ACS Catal.*, 2012, **3**, 61-73.
2. Y. Mi, J. Wang, Z. Yang, Z. Wang, H. Wang and S. Yang, *RSC Adv.*, 2014, **4**, 6060-6067.
3. D. Gerlach, M. Wimmer, R. G. Wilks, R. Félix, F. Kronast, F. Ruskea and M. Bär, *Phys. Chem. Chem. Phys.*, 2014, **16**, 26266-26272.
4. M. J. Poston, A. B. Aleksandrov, D. E. Sabo, Z. J. Zhang and T. M. Orlando, *J. Phys. Chem. C*, 2014, **118**, 12789-12795.
5. Y. Chen, H. Xia, D. Zhang, Z. Yan, F. Ouyang, X. Xiong and X. Huang, *RSC Adv.*, 2014, **4**, 8039-8043.
6. M. Jerman, Z. Qiao and D. Mergel, *Appl. Opt.*, 2005, **44**, 3006-3012.
7. Z. Li, R. Wnetrzak, W. Kwapinski and J. J. Leahy, *ACS Appl. Mater. Interfaces*, 2012, **4**, 4499-4505.
8. Y. Chen, J. Gu, D. Zhang, S. Zhu, H. Su, X. Hu, C. Feng, W. Zhang, Q. Liu and A. R. Parker, *J Mater. Chem.*, 2011, **21**, 15237-15243.
9. G. Sumana, M. Das, S. Srivastava and B. D. Malhotra, *Thin Solid Films*, 2010, **519**, 1187-1191.
10. A. Mei, X. Li, L. Liu, Z. Ku, T. Liu, Y. Rong, M. Xu, M. Hu, J. Chen, Y. Yang, M. Grätzel and H. Han, *Science*, 2014, **345**, 295-298.
11. M. T. Soo, N. Prastomo, A. Matsuda, G. Kawamura, H. Muto, A. Fauzi, M. Noor, Z. Lockman and K. Y. Cheong, *Appl. Surf. Sci.*, 2012, **258**, 5250-5258.
12. B. J. Gould, I. M. Povey, M. E. Pemble and W. R. Flavell, *J. Mater. Chem.*, 1994, **4**, 1815-1819.

13. A. Mikó, A. L. Demirel and M. Somer, *J Mater. Chem.*, 2012, **22**, 3705-3707.
14. Y. Chen, S. K. Lunsford, Y. Song, H. Ju, P. Falaras, V. likodimos, A. G. Kontos and D. D. Dionysiou, *Chem. Eng. J.*, 2011, **170**, 518-524.
15. H. A. Macleod, Thin-film Optical Filters, *Hugh Angus Macleod-Institute of Physics Publishing*, 2001.